frontiers | Frontiers in Earth Science

TYPE Original Research
PUBLISHED 08 September 2022
DOI 10.3389/feart.2022.865709

Check for updates

OPEN ACCESS

EDITED BY
Zhang Chengjun,
Lanzhou University, China

REVIEWED BY
Jianfa Chen,
China University of Petroleum, Beijing, China
Wenxia Han,
Linyi University, China

*CORRESPONDENCE
Xiaojun Zhang,
xj_zhang@petrochina.com.cn
Yongli Wang,
WYLL6800@lzb.ac.cn
Pengyuan Zhang,
zhangqlnice@163.com

SPECIALTY SECTION
This article was submitted to Geochemistry, a section of the journal Frontiers in Earth Science

RECEIVED 30 January 2022
ACCEPTED 04 August 2022
PUBLISHED 08 September 2022

CITATION
Zhang X, Zhou G, Zhang P, He Y, Wei Z, Wang G, Zhang T, He W, Ma H, Zhu C, Wei J, Ma X, Yu X, Li S, Li L and Wang Y (2022), Strontium isotope and element constraints on the paleoenvironment of the latest Ediacaran in the Sichuan Basin, southeastern Tibetan Plateau.
Front. Earth Sci. 10:865709.
doi: 10.3389/feart.2022.865709

Strontium isotope and element constraints on the paleoenvironment of the latest Ediacaran in the Sichuan Basin, southeastern Tibetan Plateau

Xiaojun Zhang[1,2]*, Gang Zhou[3], Pengyuan Zhang[4]*, Yuan He[3], Zhifu Wei[5], Gen Wang[5], Ting Zhang[5], Wei He[5], He Ma[4], Chenxi Zhu[6], Jingyi Wei[4], Xueyun Ma[5], Xiaoli Yu[5], Shangkun Li[5], Lun Li[5] and Yongli Wang[4]*

[1]PetroChina Research Institute of Petroleum Exploration & Development-Northwest (NWGI), Lanzhou, China, [2]Key Laboratory of Reservoir Description, CNPC, Lanzhou, China, [3]Exploration and Development Research Institute, PetroChina Southwest Oil and Gasfield Company, Chengdu, Sichuan, China, [4]Key Laboratory of Cenozoic Geology and Environment, Institute of Geology and Geophysics, Chinese Academy of Sciences, Beijing, China, [5]Key Laboratory of Petroleum Resources, Gansu Province/Northwest Institute of Eco−Environment and Resources, Chinese Academy of Sciences, Lanzhou, China, [6]State Key Laboratory of Petroleum Resources and Prospecting, China University of Petroleum (Beijing), Beijing, China

The Ediacaran−Cambrian period witnessed episodic extinctions, oxygenation of seawaters, Cambrian explosions, and tectonic events. However, compared with the various high-resolution geochemical records of the early−middle Ediacaran and Cambrian, the available geochemical record of the latest Ediacaran (551−542 Ma) is scarce (especially the strontium isotope and elements), which leads to the ambiguous interpretation of the paleoenvironment of the latest Ediacaran. Therefore, we conducted measurements of strontium isotopes and elemental content of a continuous series of carbonate samples from the Dengying Formation of Well PT1, located in the Sichuan Basin, southeastern Tibetan Plateau, in order to constrain the paleoenvironment of the latest Ediacaran. Strict sample screening was used to ensure that the isotopes and elements were not affected by diagenesis. Our analyses show that the environment and geochemical records of the seawater were controlled by tectonic activities, especially the Gondwana assembly. The global strontium isotope correlation indicates that the Sichuan Basin was a restricted basin (high $^{87}Sr/^{86}Sr$ values, ~0.7090), which can be attributed to the existence of a submarine high. Under the background of oxic environment, there were two episodes of anoxic expansion. During the initial stage, the stable terrigenous detrital input and oxic environment provided the prerequisite for the emergence of aerobic organisms in the restricted platform. Then, the decreasing sea level and intense tectonic activities improved the terrigenous detrital input with higher $^{87}Sr/^{86}Sr$ values (~0.7095), which stimulated the emergence of aerobic organisms, further resulting in the first episode of anoxic environment. Lastly, a global transgressive resulted in a high sea level, and thus, the Sichuan Basin changed to an open platform. The exchange with extensive oceans led to the increased paleoproductivity, which consumed oxygen and nutrients, further resulting in the second episode of anoxic environment. Thus, the restriction degree, eustatic variations, and the terrigenous detrital input affected the biological evolution and redox conditions.

KEYWORDS

strontium isotope, elements, paleoenvironment, Ediacaran Dengying Formation, Sichuan Basin

Introduction

The earth has witnessed dramatic diversification of species, episodic oxygenation of the atmosphere–ocean system, extinctions, continental rearrangement, and break-up of the supercontinent Rodinia during the Ediacaran–Cambrian (Fike et al., 2006; Schiffbauer et al., 2014; Schiffbauer, 2016; Krause et al., 2018; Zhang et al., 2018; Li et al., 2020). These geological and biological events have been recorded by geochemical signatures (Veizer et al., 1999; Anbar et al., 2007; Hardisty et al., 2017; Zhang et al., 2018; Chang et al., 2019), especially the stable carbon isotope ($\delta^{13}C$) and strontium isotopes ($^{87}Sr/^{86}Sr$) (Zhu et al., 2006; Zhu et al., 2007b; Derry, 2010). There are several prominent carbon isotope excursions during the Ediacaran–early Cambrian (Zhu et al., 2006; Zhu et al., 2007b). By contrast, there is no significant variation in the $\delta^{13}C$ record during the end Ediacaran (551–542 Ma) (Zhu et al., 2007b).

During the latest Ediacaran (551–542 Ma), the $\delta^{13}C$ values remain stable without apparent excursions, and thus, the sedimentary environment of the coeval seawater has been ignored by previous studies (Zhao et al., 2009; Wei et al., 2019). Actually, although the $\delta^{13}C$ curve of the latest Ediacaran indicates that there may be no predominant geological and biological events (Zhu et al., 2007b), this interval is the connection between the Neoproterozoic Oxygenation Event (NOE) and episodic Cambrian explosions (Chen et al., 2015; Zhang et al., 2018), which indicates the importance of this interval. Previous studies have shown that the characteristics of the seawater during the latest Ediacaran are still ambiguous (Zhang et al., 2018). Although the Ediacaran may represent the transition period when the redox condition changed from anoxic to oxic state (Sperling et al., 2015; Wood et al., 2015), the degree of oxidation and its contribution to biological diversification are uncertain (Fike et al., 2006; McFadden et al., 2008; Zhang et al., 2018). Additionally, some studies have shown that the Ediacaran seawater was the “aragonite seawater” with Mg/Ca values over 2 (Hardie, 1996, Hardie, 2003), while others proposed that the characteristics of the Ediacaran seawater may provide the precipitation condition for dolomite, indicating an “aragonite–dolomite seawater” (Hood et al., 2011; van Smeerdijk Hood and Wallace, 2012). Therefore, the sedimentary paleoenvironment of the latest Ediacaran (551–542 Ma) needs to be further restricted.

Geochemical records of chemical sedimentary rocks, especially carbonates, have been widely used in reconstructing the sedimentary paleoenvironment of the coeval seawater (Brasier et al., 1994; Maloof et al., 2010; Schiffbauer et al., 2017; Dodd et al., 2021). Although some burgeoning proxies, such as clumped-isotope (Goldberg et al., 2021), iodine (Hardisty et al., 2014), and nitrogen isotope (Chang et al., 2019), can provide more paleoenvironment information of the atmosphere–ocean system, there are still uncertainties and multiple solutions in the application of these proxies (Anbar et al., 2007; Hardisty et al., 2020). In this case, elements, stable carbon isotopes ($\delta^{13}C$), and radiogenic strontium ($^{87}Sr/^{86}Sr$) are still the most basic and reliable proxies for exploring the paleoenvironment (Derry et al., 1994; Veizer et al., 1999; Zhu et al., 2007b; Schiffbauer et al., 2017). There are many high-resolution $\delta^{13}C$ records in the latest Ediacaran globally, while the high-resolution records of elements and $^{87}Sr/^{86}Sr$ are absent (Halverson et al., 2007; Sawaki et al., 2010b; Zhang et al., 2020; Guacaneme et al., 2021). The time of Sr residence in the seawater (~2.4 Ma) (Jones and Jenkyns, 2001) is much higher than that of the mixing of seawater (10^5 years) (Jacobsen and Kaufman, 1999), leading to the global homogeneity of strontium isotope composition (Paula-Santos et al., 2015). Thus, the difference of $^{87}Sr/^{86}Sr$ values among several regions can help analyzing the relative contribution of the global and local paleoenvironment to geochemical records (Guacaneme et al., 2021). However, as $^{87}Sr/^{86}Sr$ values of carbonates are susceptible to the diagenesis, altered samples should be excluded (Marshall, 1992; Derry et al., 1994). Elements and their ratios not only can reflect the paleoenvironmental fluctuations (Riquier et al., 2006; Tribovillard et al., 2006; Algeo and Rowe, 2012; Algeo and Liu, 2020) but also can be used for determining the diagenesis (Kaufman et al., 1991; Derry, 2010). Therefore, records of $^{87}Sr/^{86}Sr$ and elements are suitable for further restricting the sedimentary environment during the latest Ediacaran (~551–542 Ma).

The Ediacaran strata is widely distributed in the Sichuan Basin, southeastern Tibetan Plateau, which is a suitable target for exploring the Ediacaran paleoenvironment (Yang et al., 2017; Hou et al., 2021; Wang et al., 2021). Therefore, we sampled Well PT1 in the Sichuan Basin in order to restrict the

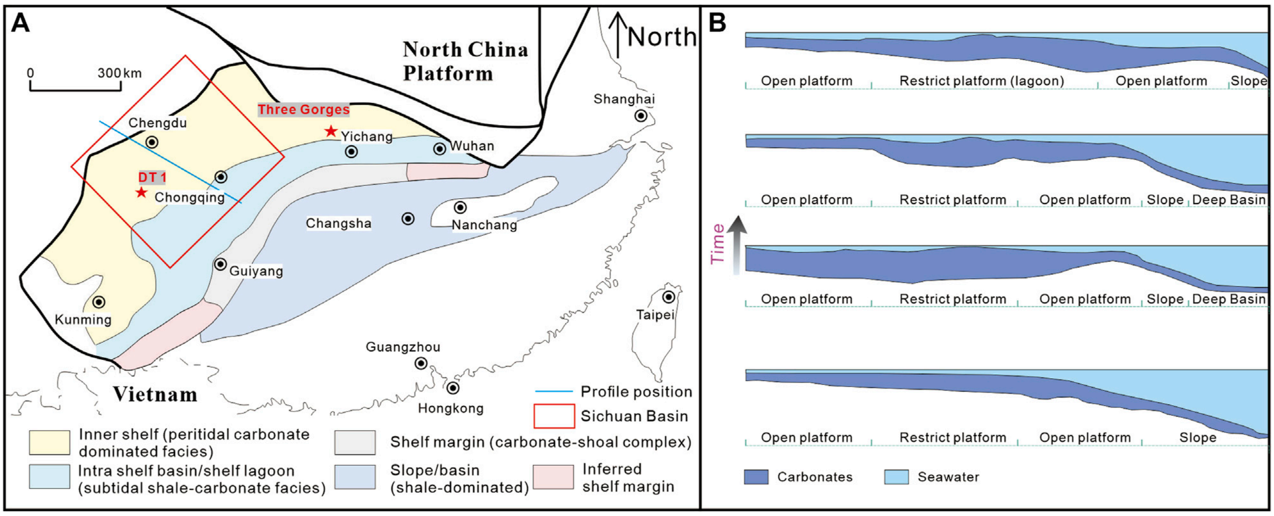

FIGURE 1
(A) Paleogeographic map of the Yangtze Block showing the location of the Sichuan Basin and Well PT1 [modified after Zhang et al. (2018), Meyer et al. (2014); Cui et al. (2016)]. **(B)** Paleogeographic evolution of the Sichuan Basin during the latest Ediacaran (551–542 Ma) (modified after Li et al. (2013), and the profile position is shown in Figure 1A).

paleoenvironment represented by the Ediacaran Dengying Formation. Our specific objectives were: 1) to provide the first set of high-resolution records of $^{87}Sr/^{86}Sr$ and elements for the latest Ediacaran (~551–542 Ma) and 2) to determine the paleoenvironmental significance of these geochemical proxies.

Geological setting

The Sichuan Basin, located in the southeastern margin of the plateau, is controlled by the fracturing of the peripheral block and tectonic movement of the basement (Li et al., 2019b; Liu et al., 2021) (Figure 1A). During the Neoproterozoic period, the Sichuan Basin belonged to the Yangtze platform (Meyer et al., 2014; Cui et al., 2016), which developed over a rifted continental margin that initiated along the southeastern side of the Yangtze block at ~800 Ma (Condon et al., 2005; Zhang et al., 2005; Li et al., 2019b; Liu et al., 2021). In the study area, the Neoproterozoic succession can be divided into three intervals: preglacial siliciclastic rocks, two Cryogenian glacial diamictite intervals, and postglacial Ediacaran marine carbonates and shales (Zhu et al., 2007a; Jiang et al., 2007). Furthermore, the Ediacaran marine carbonates and shales can be divided into the Duoshantuo Formation and Dengying Formation, respectively. The age of boundary between the Duoshantuo Formation and Dengying Formation (Zhu et al., 2007a; Jiang et al., 2007) and the Dengying Formation and its overlying Cambrian formations is 551.1 ± 0.7 Ma and ~542 Ma, respectively (Zhang et al., 1998; Jenkins et al., 2002; Condon et al., 2005; Zhang et al., 2005). The Sichuan Basin evolved to an epicontinental clastic tidal flat, to a confined platform, and then to an open platform with a gentle slope from west to east (Meyer et al., 2014; Zhang et al., 2018). According to the paleogeographic map, although the Sichuan Basin was a carbonate platform, the sedimentary environment was variable, including lagoonal facies, restricted platform, and tidal flat (Figure 1B) (Li et al., 2013b).

After the pre-Ediacaran geosyncline of the Jinning Movement and the Chengjiang Movement, the Yangtze quasi-platform began to consolidate, indicating that the block had entered the stage of platform development (Li et al., 2019b; Liu et al., 2021). The Sichuan Basin received extensive and relatively thick carbonates deposition represented by the Dengying Formation (Gao et al., 2016; Liu et al., 2021), and subsequently, the Tongwan Movement caused extensive uplift in the Sichuan Basin represented by the late Dengying Formation (Liu et al., 2021). Based on the lithology, the Dengying Formation is generally subdivided into four members: the first, second, third, and fourth member of the Dengying Formation (Deng–1, Deng–2, Deng–3, and Deng–4 Formations) from the bottom to the top (Zheng et al., 2021). The top of the Deng–2 Formation was subjected to a short period of weathering and denudation due to the first episode of the Tongwan Movement, leading to an unconformable contact between the Deng–2 and Deng–3 formations. Additionally, the second episode of the Tongwan Movement caused the overall uplift of the upper Yangtze platform, which resulted in the denudation of the Deng–4 Formation, further leading to an unconformable contact between the Deng–4 Formation and Cambrian strata (Qian et al., 2011; Hou et al., 2021).

Specifically, the lithology of the Deng–1 Formation is mainly dolomite without fungus and algae, that of the

Deng–2 Formation is algae-rich dolomite with snowflake-shaped structures and microorganisms with no snowflake-shaped structures, that of the Deng–3 Formation is mainly mudstone and classics, and that of the Deng–4 Formation is mainly algal dolomite and grey–black dolomitic mudstone (Qian et al., 2011; Hou et al., 2021).

Samples, experiments, and data presentation

Samples

A total of 118 carbonate samples of the Ediacaran Dengying Formation were selected from Well PT1 for strontium isotopic (46 samples) and elemental analyses (100 samples). Additionally, according to the lithology and paleontological characteristics of Well PT1, the carbonate samples belong to the Deng–2 Formation. Because the overlying layer of the Deng–2 Formation of Well PT1 is the Cambrian Yanjiahe Formation, it can be concluded that the Deng–3 and Deng–4 formations have been eroded.

Experiments

About 100 mg (to 0.1 mg precision) of carbonate rock materials were weighted into Savillex 7.5 ml Teflon-PFA vials and then were dissolved on a hotplate at 80°C using 2.0 ml of 0.2 M HCl for 4 h. The sample solution was cooled at room temperature for 1 h before centrifugation for 8 min at 5,000 rpm. Then, the sample solution was loaded onto the preconditioned resin column with 2 ml of AG50W × 12 (200–400 mesh) for the separation of Sr from the sample matrix. After rinsing four times with 0.5 ml of 2.5 M HCl, the column was washed with 7 ml of 5 M HCl. Afterward, the Sr fraction was stripped with 3.5 ml of 5 M HCl, and the Sr fraction was evaporated to dryness and was ready for the TIMS analysis. The Sr isotopic measurements were performed on a Thermo Fisher Triton Plus multicollector thermal ionization mass spectrometer at the Institute of Geology and Geophysics, Chinese Academy of Sciences (IGGCAS). The mass fractionation of Sr was corrected using an exponential law with $^{88}Sr/^{86}Sr$ = 8.375209. The international standard sample NBS–987 was used to evaluate instrument stability during the period of data collection. During this time, the measured average value of NBS987 was $^{87}Sr/^{86}Sr$ = 0.710,245 ± 0.000015, which is in good agreement with the reported values (Li et al., 2016; Li et al., 2019a).

All samples were crushed into fine powders greater than 200 mesh size for elemental experiments. The major and trace element concentrations were analyzed with a PANalytical MagiX PRO wavelength-dispersive X-ray fluorescence (XRF) spectrometer and Inductively Coupled Plasma Mass Spectrometer (ICP-MS), respectively, at the Northwest Branch of China Petroleum Exploration and Development Research Institute.

Results

Strontium isotopes

The $^{87}Sr/^{86}Sr$ values of the 48 measured samples range from 0.708881 to 0.710167, with a mean value of 0.709242 (Figure 2A, 3A). Vertically, the $^{87}Sr/^{86}Sr$ curve fluctuates frequently. There is a slow downward trend of the $^{87}Sr/^{86}Sr$ curve at the depth of 6,234–5,966 m, and the $^{87}Sr/^{86}Sr$ value decreases from 0.709300 to 0.708900. Then, the $^{87}Sr/^{86}Sr$ value increases rapidly, and remains stable at ~0.709400 (5,956–5,796 m). Finally, the $^{87}Sr/^{86}Sr$ curve shows a rapid drop at the depth of 5,796–5,711 m with values decreasing from 0.709500 to 0.708900.

Elements

The Sr contents are in a low level (~100 ppm) at the depth of 6,276–5,912 m and 5,866–5,726 m, and remain relatively higher (400–500 ppm) at the depth of 5,906–5,876 m (Figure 2B). The Mn/Sr values initially decrease from ~5 to ~2 at the depth of 6,276–6,206 m, and then remain stable at ~2 in the depth of 6,206–5,952 m (Figure 2C). Subsequently, there are large fluctuations at the depth of 5,952–5,866 m, and the Mn/Sr values range from ~0.5 to ~4. Finally, the Mn/Sr value decreases from ~5 to ~1.5 at the depth of 5,866–5,726 m. The CaO + MgO values share a similar trend of the Mn/Sr values (Figure 2D). The redox sensitive trace elements (RSTEs), including V, Cr, Co, and Ni, share a similar trend: initially stable at low values and then increase at the depth of 5,932–5,866 m. Finally, there is a significant increase in the trend of RSTEs at the depth of 5,800–5,700 m (Figures 3B–E). The Al_2O_3 values are at a low level (<2%), and the fluctuation of the Al_2O_3 curve is small on the whole (Figure 3F). At the depth of 6,276–5,916 m and 5,866–5,834 m, the Al_2O_3 content is almost invariable with the values of ~0.1%. By contrast, the Al_2O_3 value is relatively higher at ~0.5% and at the depth of 5,906–5,876 m. The Al_2O_3 curve fluctuates relatively intensively at the depth of 5,814–5,726 m, and shows higher values of ~0.5–2%. The TiO_2 values are at a low level (~100 ppm), and the trend of the curve is similar to that of the Al_2O_3 curve (Figure 3G).

Discussion

Diagenesis

Diagenetic processes can change the primary geochemical signatures of marine carbonates, further affecting the analysis of the coeval seawater (Kaufman et al., 1991; Derry et al., 1994). Elemental proxies have been widely used to evaluate the influence

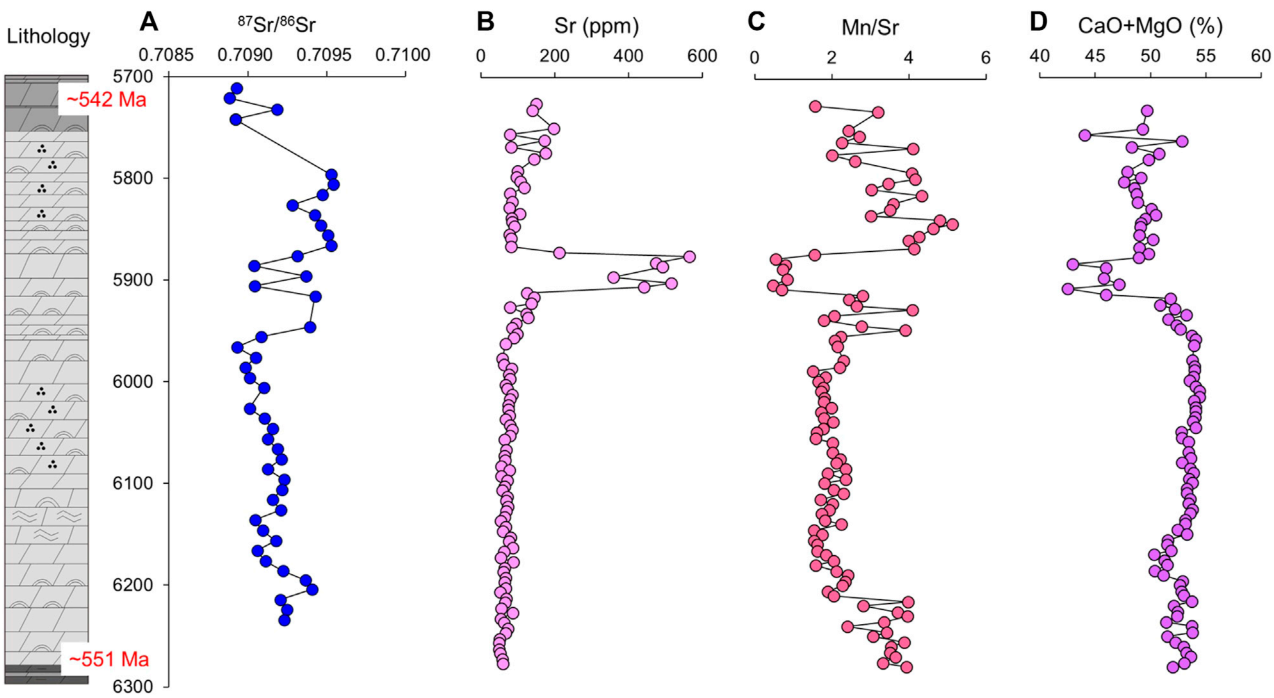

FIGURE 2
Vertical profile of $^{87}Sr/^{86}Sr$ and elements which can determine the diagenesis. **(A)** $^{87}Sr/^{86}Sr$; **(B)** Sr; **(C)** Mn/Sr; and **(D)** CaO + MgO.

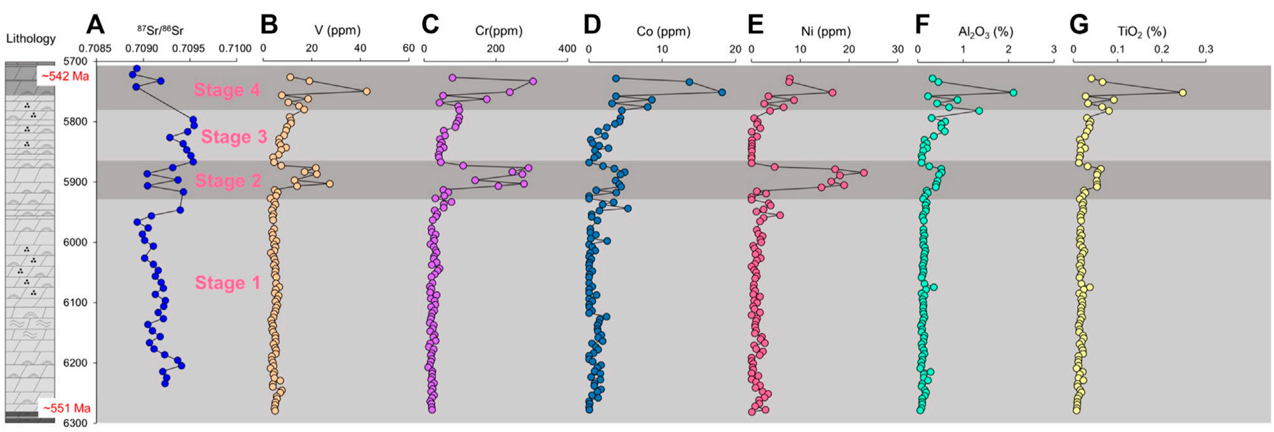

FIGURE 3
Vertical profile of $^{87}Sr/^{86}Sr$ and elements which can reconstruct the paleoenvironment. **(A)** $^{87}Sr/^{86}Sr$; **(B)** V; **(C)** Cr; **(D)** Co.; **(E)** Ni; **(F)** Al_2O_3; and **(G)** TiO_2.

of later alteration, especially the diagenesis, on the geochemical records of carbonates (Derry et al., 1994; Kaufman and Knoll, 1995). Although the traditional view is that critical values of proxies can exclude the altered samples (Derry et al., 1994), recent studies have shown that the comprehensive analysis of stable isotopes and elements rather than on the use of a fixed value is a more reasonable way to determine the diagenesis (Loyd et al., 2012; Li et al., 2013a; Schiffbauer et al., 2017). In the present study, the inner relationship and trend of multi-elemental proxies were analyzed to evaluate the diagenesis.

The loss of Sr and Na and the enrichment of Fe and Mn occur during deposition, especially under the influence of the atmospheric water cycle (Derry et al., 1994; Kaufman and Knoll, 1995; Azmy et al., 2011; Azmy et al., 2014). Therefore, the Mn/Sr ratio can be used to determine whether geochemical records of carbonates represent the original composition of seawater (Derry et al., 1994). Generally, as diagenesis becomes more severe, the Mn/Sr ratio increases and samples that have maintained the original isotopic compositions of the seawater usually have an Mn/Sr value <5 (Derry et al., 1994; Zhang et al., 2020). In addition to the sample PT1-27 (5,842 m, Mn/Sr = 5.13), Mn/Sr values of the remaining samples are less than 5, indicating that these samples may maintain the primary geochemical signatures (Figure 2C).

The Sr concentration of aragonite is <7,740 ppm in modern seawater, that of high-magnesium (Mg) calcite is 400–5,000 ppm, and that of protodolomite is 245–600 ppm (Baker and Burns, 1985). As shown in Figure 2B, based on the Sr content, samples can be divided into two groups: group 1 (5,912–6,276 m and 5,726–5,872 m), having relatively low Sr contents (<200 ppm) and group 2 (5,876–5,906 m), having relatively high Sr contents (>350 ppm). Diagenesis can reduce the Sr content of carbonate rocks to below 155 ppm (Javanbakht et al., 2018), so the Sr concentration of 155 ppm may be a critical value for excluding carbonates altered by diagenesis (Ren et al., 2019). Therefore, group 1 seems to have undergone the diagenesis, and group 2 may maintain the primary geochemical signatures. However, the Sr content of group 1 is extremely stable in intervals with different dolomite contents, indicating that the diagenesis had no prominent effect on the Sr content (Figure 2B). Actually, the Sr content of the coeval carbonates in the Tarim Basin (Ediacaran Chigebrak Formation) (~150 ppm) and the upper Yangtze Xiaotan section (Ediacaran Dengying Formation Baiyanshao Member) (<100 ppm) is also low (Li et al., 2013a; Zhang et al., 2020), indicating that Sr content is not the result of the diagenesis, but represents the original seawater composition, which further proves that a fixed critical value is not effective in some cases (Schiffbauer et al., 2017).

The samples with high purity (CaO + MgO concentrations) represent the purist carbonates which contain original $^{87}Sr/^{86}Sr$ signature (Li et al., 2013a). The (CaO + MgO) values of all samples are more than 40%, and most of the samples are more than 50%, indicating that the Dengying Formation carbonates of Well PT1 were unaffected by the diagenesis (Figure 2D). Additionally, the Rb/Sr ratio in cleaned carbonates has generally lower values than altered carbonates. In the present study, in addition to the sample PT1-27 (5,842 m, Rb/Sr = 0.16), the Rb/Sr values of the remaining samples are in a low level (Figure 4).

On the other hand, the relative relationship between these proxies was also analyzed to further exclude the altered samples (Burdett et al., 1990; Frank et al., 1997; Li et al., 2013a; Zhang et al., 2020). The location of samples in cross-plots roughly consisted with the division of samples which is based on the Sr content (Groups 1 and 2) (Figure 2B; Figure 4). Although there are good relationships between Mn/Sr and Sr (Figure 4B), CaO + MgO and Sr (Figure 4C), Mn/Sr and CaO + MgO (Figure 4E), and Rb/Sr and CaO + MgO (Figure 4F), which is presented by high coefficient of determination (R^2), the location of group 2 is clearly far from the digenetic trend, indicating that these carbonates were unaffected by the diagenesis. By contrast, one sample (PT1–27, 5,842 m) deviates from the main cluster of group 1 and has a diagenetic trend in relative to other samples, indicating that it has been altered by the diagenesis (Figures 4B–E). The cross-plots of Rb/Sr vs Sr, CaO + MgO vs Sr, Rb/Sr vs Mn/Sr, and Rb/Sr vs CaO + MgO indicates that the trend and location of group 1 show no diagenetic processes (Figures 4A,C,D,F). However, the diagenetic trend of group 1 is shown in the cross-plots of Mn/Sr vs Sr and Mn/Sr vs CaO + MgO. The inconsistency can be attributed to the low Sr content (Li et al., 2013a; Zhang et al., 2020). The low Sr content contributed to the high Mn/Sr ratios, further showing a diagenetic trend. Due to the low Sr content of seawater in the Sichuan Basin during the Ediacaran (Li et al., 2013a; Zhang et al., 2020), the use of Mn/Sr and Sr contents are obstructed. Therefore, it can be concluded that Rb/Sr and CaO + MgO values are more applicative proxies for determining the diagenesis in the present study.

Element constraints on the paleoenvironment

Biological evolution may be related to the fluctuations of the oxygen level in the ocean–atmosphere system, which shows the significance of reconstructing the redox state of seawaters (Hardisty et al., 2013; Liu et al., 2019; Wei et al., 2020; Dodd et al., 2021). Although there are various proxies for reconstructing redox condition, such as iodine (Hardisty et al., 2017; Hardisty et al., 2020), molybdenum isotope (Siebert et al., 2003), and chromium isotope (Gueguen et al., 2016), the redox-sensitive trace elements (RSTEs) are the widely used and reliable proxies (Tribovillard et al., 2006; Algeo and Tribovillard, 2009). However, the use of bimetal RSTEs, especially U/Th, V/Cr, Ni/Co, and V/(V + Ni), remains controversial (Algeo and Li, 2020; Algeo and Liu, 2020). For example, V may precipitate in the form of a stable sulfide if hydrogen sulfide is present, and Ni is related to not only the redox but also the paleoproductivity (Tribovillard et al., 2006), which may mask the true seawater environment. On the other hand, the ratio of the two elements will eliminate the true enrichment degree of the RSTEs. Therefore, in the present study, the contents of RSTEs were applied in the reconstruction of redox conditions instead of bimetal RSTEs. RSTEs tend to be more soluble in water column under a more oxic environment and enter into sediments under a more anoxic environment (Tribovillard et al., 2006; Algeo and Tribovillard, 2009; Tribovillard et al., 2012).

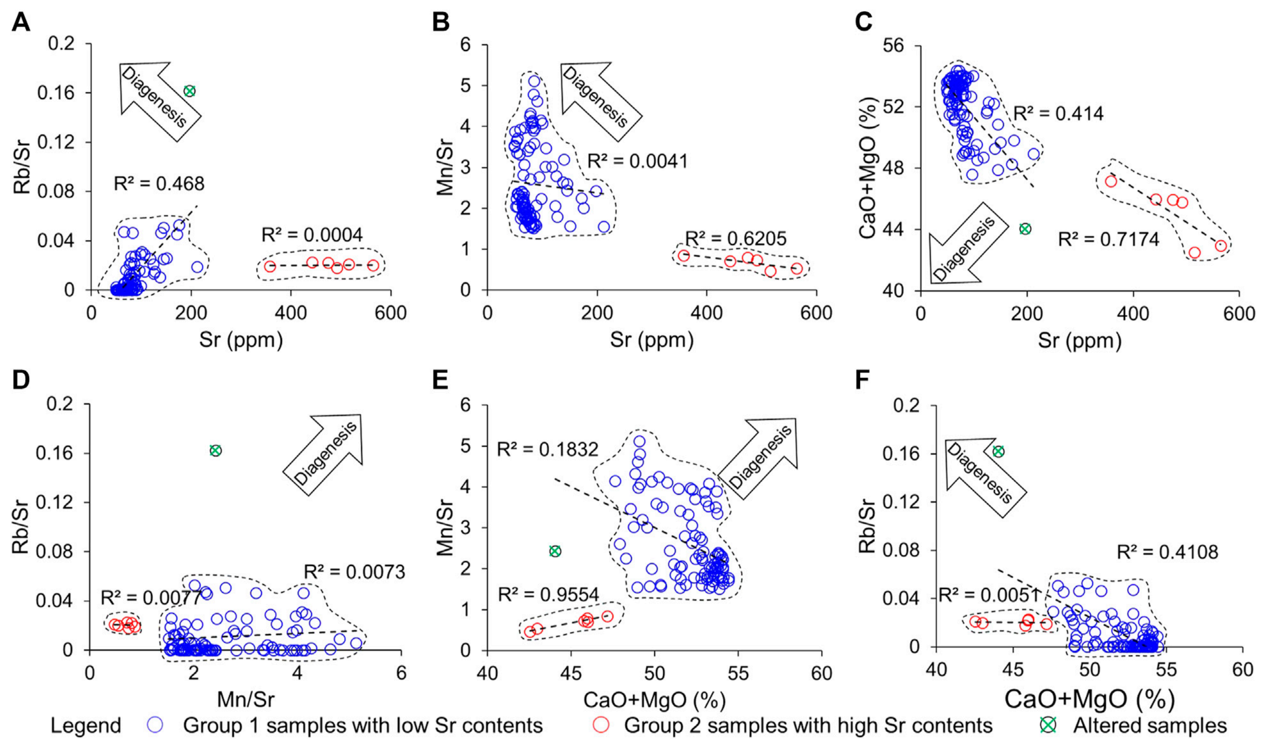

FIGURE 4
Cross-plots of **(A)** Rb/Sr vs Sr, **(B)** Mn/Sr vs Sr, **(C)** CaO + MgO vs Sr, **(D)** Rb/Sr vs Mn/Sr, **(E)** Mn/Sr vs CaO + MgO, and **(F)** Rb/Sr vs CaO + MgO.

Although the low contents of RSTEs shows that the marine environment was oxic as a whole during the latest Ediacaran (Figures 3B–E), two significant fluctuations of RSTEs indicate that there were two anoxic events. The dynamic redox condition is also supported by the δ^{238}U data (Wood et al., 2015; Zhang et al., 2018). The Fe speciation data from Newfoundland in Canada, Ce anomaly data from the Nama Group in Namibia, and Fe-S-C data from south China suggest an anoxic environment in deep water settings during the late Ediacaran (Darroch et al., 2015; Wood et al., 2015; Tostevin et al., 2016). Thus, the redox condition inferred by the contents of RSTEs indicates that the minimum oxygen zone existed in the Sichuan Basin during the Ediacaran, and there were two expansions of anoxic seawater (Figures 3B–E). Furthermore, the previous study has shown that there was an extensive marine anoxia during the terminal Ediacaran, which resulted in the decline in the Ediacaran biota from ~550 Ma (Zhang et al., 2018). Thus, fluctuations of the oxygen content may be closely related to the decline and eventual disappearance of the Ediacaran biota (Shen et al., 2008; Laflamme et al., 2013; Zhang et al., 2018).

The immobile elements, such as aluminum, zirconium, and thorium, are unaffected by weathering and diagenetic processes, and, thus, are regarded as effective proxies for the terrigenous debris input (Taylor and McLennan, 1985; Zhang et al., 2000; Tribovillard et al., 2006). Al and Ti are principally derived from aluminosilicate clay minerals, which are carried to oceans by terrigenous influx (Hayashi et al., 1997; Tribovillard et al., 2006). However, Al should not be used in cases where marine carbonates are characterized by a low detrital fraction, because excess Al may have been scavenged as hydroxides coating biogenic particles (Kryc et al., 2003). In the present study, the consistent trend of Al_2O_3 and TiO_2 suggests that it is feasible to use Al_2O_3 to represent the terrigenous detrital input (Figures 3F,G). According to the vertical trend of Al_2O_3 and TiO_2 values, the terrigenous detrital input was generally stable (Figures 2B,C). However, there were two episodes of high terrigenous detrital input, which can roughly correspond to two relatively anoxic intervals (Figure 3), indicating that there is a close relationship between the terrigenous detrital flux and redox condition. The terrigenous detrital flux is one of the sources of marine nutrients which can supply the organisms (Chang et al., 2019). In addition, the oxygen rise can stimulate biological diversification (Knoll and Carroll, 1999; Chen et al., 2015), and bioturbation and bioirrigation can affect the oxygen exchange between the surface water and the water column (Boyle et al., 2014). Therefore, during intervals of low terrigenous detrital flux, the low input of nutrients (Figure 3), such as phosphorus, indicate that less organisms demanded

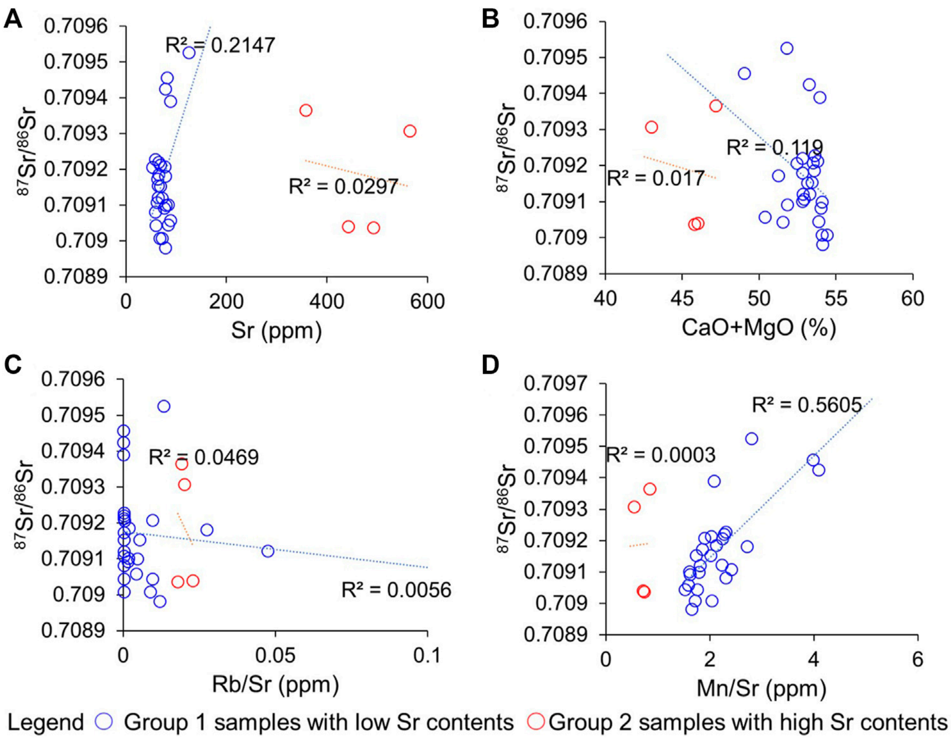

FIGURE 5
Cross-plots of **(A)** $^{87}Sr/^{86}Sr$ vs Sr, **(B)** $^{87}Sr/^{86}Sr$ vs CaO + MgO, **(C)** $^{87}Sr/^{86}Sr$ vs Rb/Sr, and **(D)** $^{87}Sr/^{86}Sr$ vs Mn/Sr.

less oxygen, leading to the depletion of the RSTEs due to the oxic environment (Figure 3). By contrast, increased nutrients supply stimulated marine productivity during intervals of high terrigenous detrital flux (Figure 3), which led to high oxygen demand on a short time scale (10^4 years), and this process would have tend to increase the ocean oxygenation on a long time scale (10^6 years) (Fike et al., 2006; Lenton et al., 2014; Cui et al., 2016; Zhang et al., 2018), resulting in the enrichment of RSTEs due to the anoxic environment.

On the other hand, there is a significant increase in the Sr content at the depth of 5,906–5,876 m, which corresponds to the interval of the first episode of high terrigenous detrital flux and anoxic environment (Figures 2B, 3). In addition, the Sr content of this interval resemble that of normal seawater, while that of 6,276–5,912 m and 5,866–5,726 m is significantly lower than that of normal seawater. However, the effect of diagenesis on the Sr content has been excluded, and thus the interval of low Sr content may indicate a local process. The position of Well PT1 was located in the shallow carbonate platform (Figure 1B), which includes lagoonal facies, restricted platform, and tidal flat, which also suggest that low Sr content may be the result of local processes. Thus, the first episode of high terrigenous detrital flux and anoxic expansion may be a local event, while the second episode may be a global event.

$^{87}Sr/^{86}Sr$ constraints on the paleoenvironment

Strontium in oceans has two main sources (Palmer and Edmond, 1989): 1) high-value strontium isotope from continental weathered rocks (global mean value of $^{87}Sr/^{86}Sr$ is 0.7119) (Peucker-Ehrenbrink and Miller, 2006) and 2) low-value strontium isotope supplied by hydrothermal exchange of mid-oceanic ridge and hydrothermal alteration of seafloor basalt (global mean value of $^{87}Sr/^{86}Sr$ is 0.7035) (Hofmann, 1997). Additionally, the diagenesis can result in elevated $^{87}Sr/^{86}Sr$ values, which can obscure the real $^{87}Sr/^{86}Sr$ signature (Derry et al., 1994). For example, the global strontium isotope composition of oceans during the Cambrian–Toyonian is 0.708,853–0.709,667 (Zhang et al., 2022), while the $^{87}Sr/^{86}Sr$ value of coeval altered carbonates exceed 0.710,300 (Fu et al., 2020). Due to the lack of high-precision $^{87}Sr/^{86}Sr$ records, the strontium isotope composition of the Ediacaran seawater has not been well-limited (Halverson et al., 2007; Sawaki et al., 2010a; Guacaneme et al., 2021). Therefore, the identification of the diagenesis and global comparison of $^{87}Sr/^{86}Sr$ values during the interval presented by the Ediacaran Dengying Formation are necessary.

Although altered samples have been excluded, the influence of the diagenesis on the strontium isotope composition is still

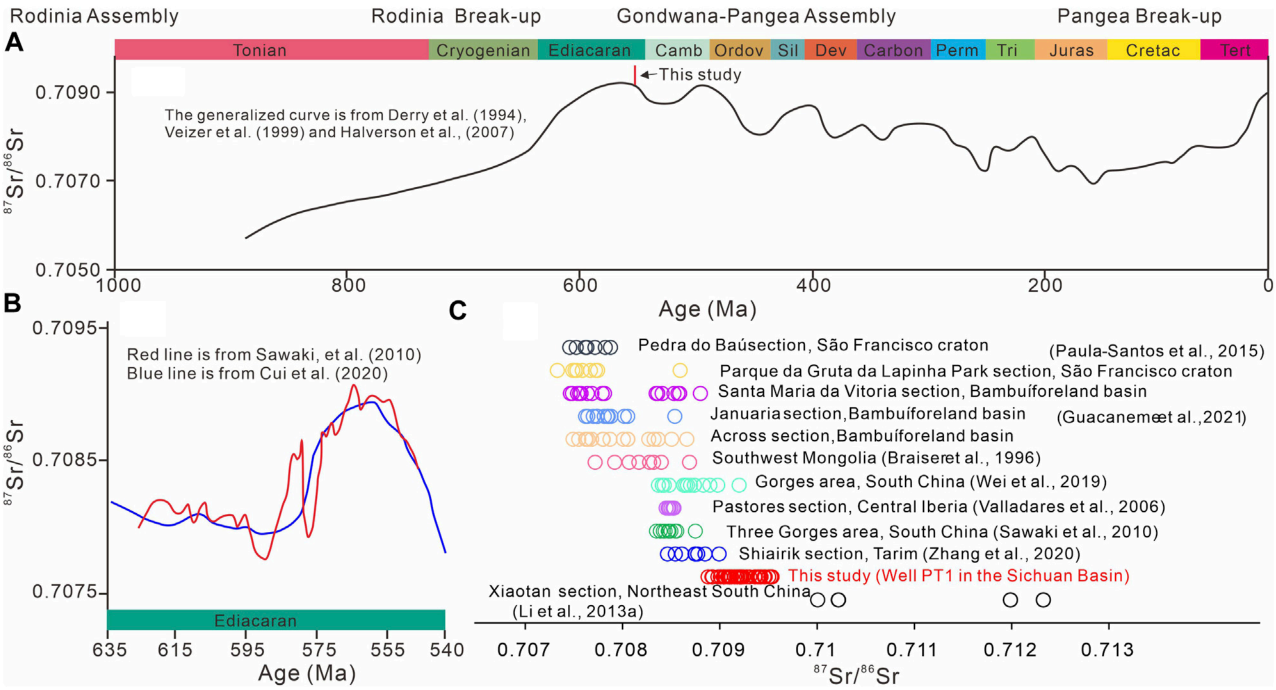

FIGURE 6
(A) Record of marine $^{87}Sr/^{86}Sr$ over the past 1,000 Ma (modified after Derry et al. (1994), Veizer et al. (1999) and Halverson et al. (2007); **(B)** record of marine $^{87}Sr/^{86}Sr$ during the Ediacaran [the red line is from Sawaki et al. (2010b), and the yellow line is from Cui et al. (2020)]; **(C)** range of $^{87}Sr/^{86}Sr$ values of the Dengying Formation and coeval other formations (the data of south China is from Li et al. (2013a) and Wei et al. (2019); the data of the Tarim Basin is from Zhang et al. (2020); the data of central Iberia is from Valladares et al. (2006); the data of southwest Mongolia is from Braiser et al. (1996); the data of the Bambuí foreland basin is from Guacaneme et al. (2021); the data of the southern São Francisco craton is from Paula-Santos et al. (2015).

evaluated in order to avoid possible interferences. As shown in the cross-plots of $^{87}Sr/^{86}Sr$ vs Sr, $^{87}Sr/^{86}Sr$ vs Rb/Sr, and $^{87}Sr/^{86}Sr$ vs CaO + MgO, there is no obvious correlation between these proxies and $^{87}Sr/^{86}Sr$ (Figures 5–D), which is presented by the low values of the coefficient of determination (R^2), indicating that the diagenesis unaffected the strontium isotope composition. The $^{87}Sr/^{86}Sr$ values and Mn/Sr ratios show a positive relationship, which can be attributed to the low Sr content of the Ediacaran seawater as previously mentioned (Li et al., 2013a; Zhang et al., 2020). Thus, our high $^{87}Sr/^{86}Sr$ values can be used to restrict the sedimentary environment of the Sichuan Basin during the interval presented by the Deng-2 Formation.

The strontium isotope values of the latest Ediacaran (551–542 Ma) in the present study (Figure 2A) are high in both long and short scales (Figures 6A,B) (Derry et al., 1994; Veizer et al., 1999; Halverson et al., 2007; Cui et al., 2020). Moreover, the global correlation of the late Ediacaran $^{87}Sr/^{86}Sr$ records show that in addition to the extremely high $^{87}Sr/^{86}Sr$ values of the Xiaotan section in south China (0.710,007–0.712,326) which has been attributed to the diagenesis (Li et al., 2013a), the $^{87}Sr/^{86}Sr$ values of Well PT1 are significantly higher than that of other coeval records (Figure 2A), such as the low $^{87}Sr/^{86}Sr$ values of the Tsagaan Oloom Formation in southwest Mongolia (0.70772–0.70869) (Brasier et al., 1996), the Sete Lagoas Formation in the Bambuí foreland Basin (0.707493–0.708663) (Guacaneme et al., 2021), and Bambuí Group in southern São Francisco (0.707332–0.708878) (Paula-Santos et al., 2015), and moderate $^{87}Sr/^{86}Sr$ values of the Chigebrak Formation in the Tarim Basin (0.708464–0.708994) (Zhang et al., 2020), unit-4 layer in central Iberia (0.70845–0.70875) (Valladares et al., 2006) and the Dengying Formation in Gorges area, South China (0.70835–0.70875) (Sawaki et al., 2010b; Wei et al., 2019) (Figure 6C). These low $^{87}Sr/^{86}Sr$ values (<0.7085) have been interpretated as the result of the local process rather than the global signature, while moderate $^{87}Sr/^{86}Sr$ values (0.7085–0.7090) have been regarded as the global signature (Paula-Santos et al., 2015; Guacaneme et al., 2021). During the Ediacaran, the Gondwana assembly and related marginal orogenesis caused paleogeographic changes, which led to marine isolation and unique geochemical characteristics (Li et al., 2008; Li et al., 2013c; Wei et al., 2019). A modern case also indicates the importance of tectonic activities on the geochemical characteristics: the uplifts of the Himalaya and Tibetan

10.3389/feart.2022.865709

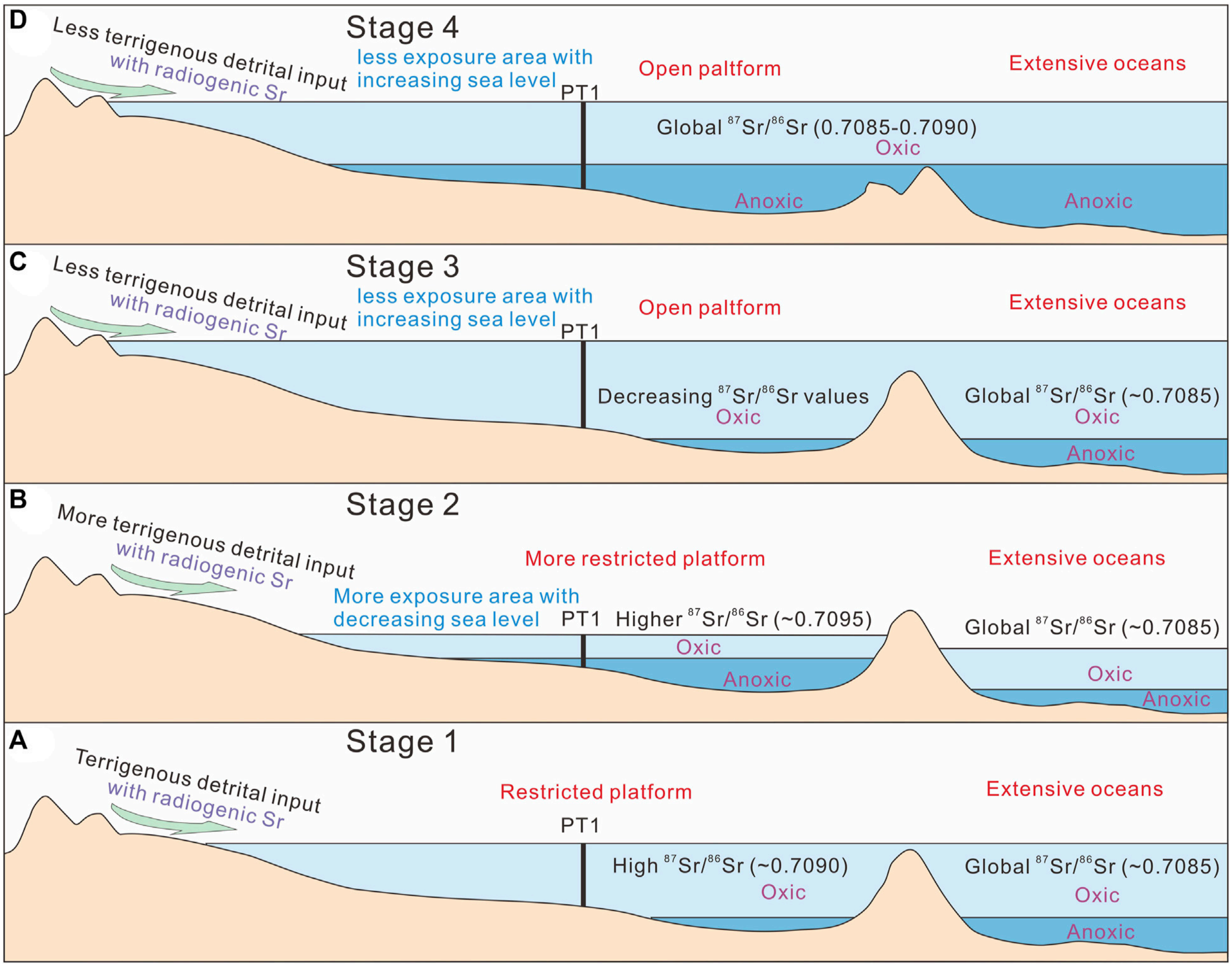

FIGURE 7
Evolution of the geochemical records and paleoenvironment during the latest Ediacaran in the Sichuan Basin. **(A)** Stage 1; **(B)** stage 2; **(C)** stage 3; and **(D)** stage 4.

Plateau increased the continental weathering rates, leading to more input of radiogenic Sr isotope to oceans (Richter et al., 1992). Furthermore, the seawaters of near-shore basins were commonly flooded with continental freshwater with little chance to exchange with global seawaters (Frimmel, 2009).

In the case of excluding the effect of the diagenesis, the evidently high $^{87}Sr/^{86}Sr$ values of this study may be also the result of local processes (Figure 2A), which is consistent with the analyses of elements. Combined with the paleogeographic information (Figure 1), it can be concluded that the sedimentary environment of the Sichuan Basin may be restricted during the latest Ediacaran, such as lagoonal facies and restricted platform (Figure 1B). The high $^{87}Sr/^{86}Sr$ values also suggest the relatively high terrigenous detrital input from continental weathering (Peucker-Ehrenbrink and Miller, 2006; Zhao et al., 2009), and reduced contribution of oceanic hydrothermal sources to $^{87}Sr/^{86}Sr$ values (Hofmann, 1997). During the late Ediacaran, the assembly of Gondwana was still in process, indicating a period of intense tectonic activities. Thus, the widespread continental collision caused high topographic landscape, indicating intense continental weathering (Richter et al., 1992; Li et al., 2008; Li et al., 2013c). In addition, when the sea level falls, a large continental area is exposed for weathering, resulting in the increased supply of terrigenous material to the ocean (Palmer and Edmond, 1989; Hofmann, 1997). Therefore, the intense continental weathering and low sea level resulted in the increased supply of terrigenous strontium to the Sichuan Basin during the Ediacaran, further leading to high $^{87}Sr/^{86}Sr$ values (Figure 2A).

On the other hand, the Three Gorges area was also located in the upper Yangtze Platform (Sawaki et al., 2010b; Zhang et al., 2018; Wei et al., 2019), so carbonates of Well PT1 and the Three Gorges area should share similar $^{87}Sr/^{86}Sr$ values due to the homogeneity of strontium isotope composition (Jacobsen and Kaufman, 1999; Paula-Santos et al., 2015). However, the strontium isotope composition of the Three Gorges area (0.70835–0.70875) is similar with the extensive oceans, while that of well PT1 is higher than that of the extensive oceans. The paleogeographic position of PT1 and Three Gorges area shows that the position of Three Gorges area was closer to extensive oceans than that of Well PT1 (Figure 1A) (Zhang et al., 2018). Therefore, we inferred that there was a high submarine in the Sichuan Basin, restricting the exchange of water between the seawater of Sichuan Basin and the extensive oceans, which resembles the case of the late Miocene Mediterranean marine basin (Schildgen et al., 2014). In this case, due to the existence of the high submarine, the input of the terrigenous debris into the location of Well PT1 was more than that of Three Gorges area, which led to more radiogenic Sr in the seawater of the location of Well PT1. Thus, the $^{87}Sr/^{86}Sr$ record of the Three Gorges area of south China can represent the global strontium isotope composition (Valladares et al., 2006; Sawaki et al., 2010b; Wei et al., 2019), while that in the Sichuan Basin was a local process.

The vertical fluctuations of the $^{87}Sr/^{86}Sr$ values may be fundamentally controlled by the Gondwana assembly (Li et al., 2008; Li et al., 2013c). The Gondwana assembly controlled the continental exposure area and continental weathering intensity, further affecting the terrigenous detrital input and driving the restriction degree of the Sichuan Basin by controlling tectonic uplifts. According to the vertical trends of elements and $^{87}Sr/^{86}Sr$ values (Figure 2A), the sedimentary environment of the Sichuan Basin during the latest Ediacaran can be divided into four stages. During stage 1, the terrigenous detrital input was stable, which presented stable TiO_2, Al_2O_3, and Sr contents. Low Sr contents and high $^{87}Sr/^{86}Sr$ values indicate the restricted exchange with extensive oceans, and thus the Sichuan Basin is a restricted platform (Figure 7A). The long-term oxic environment and nutrients supply during stage 1 provided the prerequisite for the emergence of aerobic organisms in stage 2. During stage 2, the Gondwana assembly resulted in intense tectonic activity and low sea level (more exposed area), further leading to the increased terrigenous detrital input, which is presented by high $^{87}Sr/^{86}Sr$ values (0.7093–0.7095) (Figure 7B). The increased terrigenous detrital input stimulated the emergence of aerobic organisms, which consumed the previously stored oxygen, leading to the first episode of anoxic environment. During stage 3, the Gondwana assembly was still in process (Li et al., 2008; Li et al., 2013c), causing the continuous increase of the terrigenous detrital input. However, the $^{87}Sr/^{86}Sr$ and Sr values decreased, which may have resulted from global transgression. The rising sea level led to the mixture of the seawater of the Sichuan Basin and extensive oceans, further resulting in the decline of the $^{87}Sr/^{86}Sr$ values (Figure 7C). The high sea level provided upwellings which carried enough nutrients, stimulating the paleoproductivity. Thus, the increased paleoproductivity consumed oxygen and nutrients, furthering resulting in the second episode of anoxic environment in stage 4 (Figure 7D).

Conclusion

The determination of the effect of the diagenesis on carbonates should depend on the relationships between multiproxies, such as Mn/Sr, Rb/Sr, and Sr values, rather than critical values of these proxies.

The records of element and strontium isotopes show the tectonically induced strontium isotope and elemental changes in the Ediacaran seawater. During the latest Ediacaran, the Gondwana assembly was in process, which controlled the continental exposure by regulating the sea level, further affecting the terrigenous detrital input. Simultaneously, the degree of the basin restriction was driven by the Gondwana assembly by controlling tectonic uplifts and the sea level. The terrigenous detrital input and the degree of the basin restriction further affected oceanic organisms and redox conditions.

The paleoenvironment of the Sichuan Basin during the latest Ediacaran can be divided in to four stages. During stage 1, the stable terrigenous detrital input and oxic environment provided the prerequisite for the emergence of aerobic organisms. With the intense tectonic uplifts and the decreasing sea level caused by the Gondwana assembly, the Sichuan Basin was more restricted during stage 2. The increased terrigenous detrital input stimulated the emergence of aerobic organisms, which consumed the previous stored oxygen, leading to the first episode of anoxic environment. During stage 3, a transgression led to the mixture of the seawater of the Sichuan Basin and extensive oceans. As a result, the Sichuan Basin changed from a restricted platform to an open one. The high sea level provided enough nutrients, which led to increased paleoproductivity. Thus, the high paleoproductivity consumed oxygen and nutrients, resulting in the second episode of anoxic environment.

Data availability statement

The original contributions presented in the study are included in the article/Supplementary Material. Further inquiries can be directed to the corresponding authors.

Author contributions

XZ: conceptualization, supervision, writing, and modifications. GZ: methodology, modifications software, and

10.3389/feart.2022.865709

drawing. PZ: methodology, sample collection, writing, and modifications. YH: modifications, reviewing, and editing and drawing. ZW: methodology, reviewing, and editing. GW: software and visualization. TZ: supervision and investigation. WH: investigation. HM: software and validation. CZ: visualization, software, and drawing. JW: writing, reviewing, and editing. XM: investigation. XY: reviewing and investigation. SL: software and editing. LL: sample collection. YW: conceptualization, supervision, reviewing, and editing.

Funding

This work was supported by the National Natural Science Foundation of China (grant number 41831176), the Third Xinjiang Scientific Expedition Program (grant number 2021XJKK1103), the Second Tibetan Plateau Scientific Expedition and Research (STEP) Program (grant number 2019QZKK0707), the Strategic Priority Research Program of CAS (grant numberXDB26000000), the National Natural Science Foundation of China (grant numbers 41902028, 41972030, and 42072038), the National Key R and D Program of China (grant number2017YFA0604803), the CAS "Light of West China" Program, and the Youth Innovation Promotion Association CAS (No.2021425).

Conflict of interest

Author XZ was employed by CNPC. Authors GZ and YH were employed by Petro China Southwest Oil and Gasfield Company.

The remaining authors declare that the research was conducted in the absence of any commercial or financial relationships that could be construed as a potential conflict of interest.

Publisher's note

All claims expressed in this article are solely those of the authors and do not necessarily represent those of their affiliated organizations, or those of the publisher, the editors, and the reviewers. Any product that may be evaluated in this article, or claim that may be made by its manufacturer, is not guaranteed or endorsed by the publisher.

Supplementary material

The Supplementary Material for this article can be found online at: https://www.frontiersin.org/articles/10.3389/feart.2022.865709/full#supplementary-material

References

Algeo, T. J., and Li, C. (2020). Redox classification and calibration of redox thresholds in sedimentary systems. *Geochimica Cosmochimica Acta* 287, 8–26. doi:10.1016/j.gca.2020.01.055

Algeo, T. J., and Liu, J. (2020). A re–assessment of elemental proxies for paleoredox analysis. *Chem. Geol.* 540, 119549. doi:10.1016/j.chemgeo.2020.119549

Algeo, T. J., and Rowe, H. (2012). Paleoceanographic applications of trace–metal concentration data. *Chem. Geol.* 324–325, 6–18. doi:10.1016/j.chemgeo.2011.09.002

Algeo, T. J., and Tribovillard, N. (2009). Environmental analysis of paleoceanographic systems based on molybdenum–uranium covariation. *Chem. Geol.* 268, 211–225. doi:10.1016/j.chemgeo.2009.09.001

Anbar, A. D., Duan, Y., Lyons, T. W., Arnold, G. L., Kendall, B., Creaser, R. A., et al. (2007). A whiff of oxygen before the great oxidation event? *Science* 317, 1903–1906. doi:10.1126/science.1140325

Azmy, K., Brand, U., Sylvester, P., Gleeson, S. A., Logan, A., and Bitner, M. A. (2011). Biogenic and abiogenic low–Mg calcite (bLMC and aLMC): Evaluation of seawater–REE composition, water masses and carbonate diagenesis. *Chem. Geol.* 280, 180–190. doi:10.1016/j.chemgeo.2010.11.007

Azmy, K., Stouge, S., Brand, U., Bagnoli, G., and Ripperdan, R. (2014). High–resolution chemostratigraphy of the Cambrian–Ordovician GSSP: Enhanced global correlation tool. *Palaeogeogr. Palaeoclimatol. Palaeoecol.* 409, 135–144. doi:10.1016/j.palaeo.2014.05.010

Baker, P. A., and Burns, S. J. (1985). Occurrence and formation of dolomite in organic–rich continental margin sediments. *AAPG Bull.* 69, 1917–1930. doi:10.1306/94885570-1704-11D7-8645000102C1865D

Boyle, R. A., Dahl, T. W., Dale, A. W., Shields–Zhou, G. A., Zhu, M., Brasier, M. D., et al. (2014). Stabilization of the coupled oxygen and phosphorus cycles by the evolution of bioturbation. *Nat. Geosci.* 7, 671–676. doi:10.1038/ngeo2213

Brasier, M. D., Corfield, R. M., Deryy, L. A., Rozanov, A. Y., and Zhuravlev, A. Y. (1994). Multiple $\delta^{13}C$ excursions spanning the Cambrian explosion to the Botomian crisis in Siberia. *Geol.* 22, 455–458. doi:10.1130/0091-7613(1994)022<0455:mcestc>2.3.co;2

Brasier, M., Shields, G., Kuleshov, V., and Zhegallo, E. J. G. M. (1996). Integrated chemo–and biostratigraphic calibration of early animal evolution: Neoproterozoic–early Cambrian of southwest Mongolia. *Geol. Mag.* 133, 445–485. doi:10.1017/s0016756800007603

Burdett, W. J., Grotzinger, J. P., and Arthur, M. A. (1990). Did major changes in the stable–isotope composition of Proterozoic seawater occur? *Geol.* 18, 227–230. doi:10.1130/0091-7613(1990)018<0227:dmcits>2.3.co;2

Chang, C., Hu, W., Wang, X., Huang, K.–J., Yang, A., and Zhang, X. (2019). Nitrogen isotope evidence for an oligotrophic shallow ocean during the Cambrian Stage 4. *Geochimica Cosmochimica Acta* 257, 49–67. doi:10.1016/j.gca.2019.04.021

Chen, X., Ling, H. F., Vance, D., ShieldsZhou, G. A., Zhu, M., Poulton, S. W., et al. (2015). Rise to modern levels of ocean oxygenation coincided with the Cambrian radiation of animals. *Nat. Commun.* 6, 7142. doi:10.1038/ncomms8142

Condon, D., Zhu, M., Bowring, S., Wang, W., Yang, A., and Jin, Y. (2005). U–Pb ages from the neoproterozoic doushantuo formation, China. *Science* 308, 95–98. doi:10.1126/science.1107765

Cui, J., Huang, J., and Xie, S. (2008). Characterstics of seasonal variations of leaf n -alkanes and n -alkenes in modern higher plants in Qingjiang, Hubei Province, China. *Sci. Bull.* 53 (11), 1318–1323. doi:10.1007/s11434-008-0194-8

Cui, H., Kaufman, A. J., Xiao, S., Peek, S., Cao, H., Min, X., et al. (2016). Environmental context for the terminal Ediacaran biomineralization of animals. *Geobiology* 14, 344–363. doi:10.1111/gbi.12178

Darroch, S. A., Sperling, E. A., Boag, T. H., Racicot, R. A., Mason, S. J., Morgan, A. S., et al. (2015). Biotic replacement and mass extinction of the Ediacara biota. *Proc. R. Soc. B Biol. Sci.* 282, 20151003. doi:10.1098/rspb.2015.1003

Derry, L. A. (2010). A burial diagenesis origin for the Ediacaran Shuram–Wonoka carbon isotope anomaly. *Earth Planet. Sci. Lett.* 294, 152–162. doi:10.1016/j.epsl.2010.03.022

Derry, L. A., Brasier, M. D., Corfield, R. M., Rozanov, A. Y., and Zhuravlev, A. Y. (1994). Sr and C isotopes in lower cambrian carbonates from the siberian craton: A paleoenvironmental record during the 'cambrian explosion. *Earth Planet. Sci. Lett.* 128, 671–681. doi:10.1016/0012-821x(94)90178-3

Dodd, M. S., Zhang, Z., Li, C., Algeo, T. J., Lyons, T. W., Hardisty, D. S., et al. (2021). Development of carbonate–associated phosphate (CAP) as a proxy for reconstructing ancient ocean phosphate levels. *Geochimica Cosmochimica Acta* 301, 48–69. doi:10.1016/j.gca.2021.02.038

Fike, D. A., Grotzinger, J. P., Pratt, L. M., and Summons, R. E. (2006). Oxidation of the ediacaran ocean. *Nature* 444, 744–747. doi:10.1038/nature05345

Frank, T. D., Lyons, T. W., and Lohmann, K. C. (1997). Isotopic evidence for the paleoenvironmental evolution of the mesoproterozoic helena formation, belt supergroup, Montana, USA. *Geochimica Cosmochimica Acta* 61, 5023–5041. doi:10.1016/s0016-7037(97)80341-9

Frimmel, H. E. J. C. G. (2009). Trace element distribution in Neoproterozoic carbonates as palaeoenvironmental indicator. *Chem. Geol.* 258, 338–353. doi:10.1016/j.chemgeo.2008.10.033

Fu, Q., Hu, S., Xu, Z., Zhao, W., Shi, S., and Zeng, H. (2020). Depositional and diagenetic controls on deeply buried Cambrian carbonate reservoirs: Longwangmiao Formation in the Moxi–Gaoshiti area, Sichuan Basin, southwestern China. *Mar. Petroleum Geol.* 117, 104318. doi:10.1016/j.marpetgeo.2020.104318

Gao, R., Chen, C., Wang, H., Lu, Z., Brown, L., Dong, S., et al. (2016). SINOPROBE deep reflection profile reveals a Neo–Proterozoic subduction zone beneath Sichuan Basin. *Earth Planet. Sci. Lett.* 454, 86–91. doi:10.1016/j.epsl.2016.08.030

Goldberg, S. L., Present, T. M., Finnegan, S., and Bergmann, K. D. (2021). A high–resolution record of early Paleozoic climate. *Proc. Natl. Acad. Sci. U. S. A.* 118, e2013083118. doi:10.1073/pnas.2013083118

Guacaneme, C., Babinski, M., Bedoya–Rueda, C., Paula–Santos, G. M., Caetano–Filho, S., Kuchenbecker, M., et al. (2021). Tectonically–induced strontium isotope changes in ancient restricted seas: The case of the Ediacaran–Cambrian Bambuí foreland basin system, east Brazil. *Gondwana Res.* 93, 275–290. doi:10.1016/j.gr.2021.02.007

Gueguen, B., Reinhard, C. T., Algeo, T. J., Peterson, L. C., Nielsen, S. G., Wang, X., et al. (2016). The chromium isotope composition of reducing and oxic marine sediments. *Geochim. Cosmochim. Acta* 184, 1–19. doi:10.1016/j.gca.2016.04.004

Halverson, G. P., Dudás, F. Ö., Maloof, A. C., and Bowring, S. A. (2007). Evolution of the 87Sr/86Sr composition of Neoproterozoic seawater. *Palaeogeogr. Palaeoclimatol. Palaeoecol.* 256, 103–129. doi:10.1016/j.palaeo.2007.02.028

Hardie, L. A. (1996). Secular variation in seawater chemistry: An explanation for the coupled secular variation in the mineralogies of marine limestones and potash evaporites over the past 600 m.y. *Geol.* 24, 279–283. doi:10.1130/0091-7613(1996)024<0279:svisca>2.3.co;2

Hardie, L. A. (2003). Secular variations in Precambrian seawater chemistry and the timing of Precambrian aragonite seas and calcite seas. *Geol.* 31, 785–788. doi:10.1130/g19657.1

Hardisty, D. S., Horner, T. J., Wankel, S. D., Blusztajn, J., and Nielsen, S. G. (2020). Experimental observations of marine iodide oxidation using a novel sparge–interface MC–ICP–MS technique. *Chem. Geol.* 532, 119360. doi:10.1016/j.chemgeo.2019.119360

Hardisty, D. S., Lu, Z., Bekker, A., Diamond, C. W., Gill, B. C., Jiang, G., et al. (2017). Perspectives on Proterozoic surface ocean redox from iodine contents in ancient and recent carbonate. *Earth Planet. Sci. Lett.* 463, 159–170. doi:10.1016/j.epsl.2017.01.032

Hardisty, D. S., Lu, Z., Planavsky, N. J., Bekker, A., Philippot, P., Zhou, X., et al. (2014). An iodine record of Paleoproterozoic surface ocean oxygenation. *Geology* 42, 619–622. doi:10.1130/g35439.1

Hardisty, D. S., Olyphant, G. A., Bell, J. B., Johnson, A. P., and Pratt, L. M. (2013). Acidophilic sulfur disproportionation. *Geochimica Cosmochimica Acta* 113, 136–151. doi:10.1016/j.gca.2013.03.013

Hayashi, K. I., Fujisawa, H., Holland, H. D., and Ohmoto, H. (1997). Geochemistry of ~1.9 Ga sedimentary rocks from northeastern Labrador, Canada. *Geochimica Cosmochimica Acta* 61, 4115–4137. doi:10.1016/s0016-7037(97)00214-7

Hofmann, A. W. (1997). Mantle geochemistry the message from oceanic volcanism. *Nature* 385, 219–229. doi:10.1038/385219a0

Hood, A. v. S., Wallace, M. W., and Drysdale, R. N. (2011). Neoproterozoic aragonite–dolomite seas? Widespread marine dolomite precipitation in cryogenian reef complexes. *Geology* 39, 871–874. doi:10.1130/g32119.1

Hou, L., Yang, F., Yang, C., and Wang, J. (2021). Characteristics and Formation of sinian (ediacaran) carbonate karstic reservoirs in Dengying Formation in Sichuan Basin, China. *Petroleum Res.* 6, 144–157. doi:10.1016/j.ptlrs.2020.11.003

Jacobsen, S. B., and Kaufman, A. J. (1999). The Sr, C and O isotopic evolution of Neoproterozoic seawater. *Chem. Geol.* 161, 37–57. doi:10.1016/s0009-2541(99)00080-7

Javanbakht, M., Wanas, H. A., Jafarian, A., Shahsavan, N., and Sahraeyan, M. (2018). Carbonate diagenesis in the barremian–aptian tirgan formation (Kopet–Dagh basin, NE Iran): Petrographic, geochemical and reservoir quality constraints. *J. Afr. Earth Sci.* 144, 122–135. doi:10.1016/j.jafrearsci.2018.04.016

Jenkins, R. J. F., Cooper, J. A., and Compston, W. (2002). Age and biostratigraphy of Early Cambrian tuffs from SE Australia and southern China. *J. Geol. Soc. Lond.* 159, 645–658. doi:10.1144/0016-764901-127

Jiang, G., Kaufman, A. J., Christie–Blick, N., Zhang, S., Wu, H. J. E., and Letters, P. S. (2007). Carbon isotope variability across the Ediacaran Yangtze platform in South China: Implications for a large surface–to–deep ocean δ13C gradient. *Earth Planet. Sci. Lett.* 261, 303–320. doi:10.1016/j.epsl.2007.07.009

Jones, C. E., and Jenkyns, H. C. (2001). Seawater strontium isotopes, oceanic anoxic events, and seafloor hydrothermal activity in the jurassic and cretaceous. *Am. J. Sci.* 301, 112–149. doi:10.2475/ajs.301.2.112

Kaufman, A. J., Hayes, J. M., Knoll, A. H., and Germs, G. J. B. (1991). Isotopic compositions of carbonates and organic carbon from upper Proterozoic successions in Namibia, stratigraphic variation and the effects of diagenesis and metamorphism. *Precambrian Res.* 49, 301–327. doi:10.1016/0301-9268(91)90039-d

Kaufman, A. J., and Knoll, A. H. (1995). Neoproterozoic variations in the C isotopic composition of seawater stratigraphic and biogeochemical implications. *Precambrian Res.* 73, 27–49. doi:10.1016/0301-9268(94)00070-8

Knoll, A. H., and Carroll, S. B. (1999). Early animal evolution: Emerging views from comparative biology and geology. *Science* 284, 2129–2137. doi:10.1126/science.284.5423.2129

Krause, A. J., Mills, B. J. W., Zhang, S., Planavsky, N. J., Lenton, T. M., and Poulton, S. W. (2018). Stepwise oxygenation of the Paleozoic atmosphere. *Nat. Commun.* 9, 4081. doi:10.1038/s41467-018-06383-y

Kryc, K. A., Murray, R. W., and Murray, D. W. (2003). Al–to–oxide and Ti–to–organic linkages in biogenic sediment: Relationships to paleo–export production and bulk Al/Ti. *Earth Planet. Sci. Lett.* 211, 125–141. doi:10.1016/s0012-821x(03)00136-5

Laflamme, M., Darroch, S. A. F., Tweedt, S. M., Peterson, K. J., and Erwin, D. H. (2013). The end of the Ediacara biota: Extinction, biotic replacement, or Cheshire Cat? *Gondwana Res.* 23, 558–573. doi:10.1016/j.gr.2012.11.004

Lenton, T. M., Boyle, R. A., Poulton, S. W., Shields–Zhou, G. A., and Butterfield, N. J. J. N. G. (2014). Co–evolution of eukaryotes and ocean oxygenation in the Neoproterozoic era. *Nat. Geosci.* 7, 257–265. doi:10.1038/ngeo2108

Li, C. F., Wang, X. C., Guo, J. H., Chu, Z. Y., and Feng, L. J. (2016). Rapid separation scheme of Sr, Nd, Pb, and Hf from a single rock digest using a tandem chromatography column prior to isotope ratio measurements by mass spectrometry. *J. Anal. At. Spectrom.* 31, 1150–1159. doi:10.1039/c5ja00477b

Li, C. F., Wu, H. Q., Chu, Z. Y., Wang, X. C., Li, Y. L., and Guo, J. H. (2019a). Precise determination of radiogenic Sr and Nd isotopic ratios and Rb, Sr, Sm, Nd elemental concentrations in four coal ash and coal fly ash reference materials using isotope dilution thermal ionization mass spectrometry. *Microchem. J.* 146, 906–913. doi:10.1016/j.microc.2019.02.034

Li, C., Shi, W., Cheng, M., Jin, C., and Algeo, T. J. (2020). The redox structure of Ediacaran and early Cambrian oceans and its controls. *Sci. Bull.* 65, 2141–2149. doi:10.1016/j.scib.2020.09.023

Li, D., Ling, H. F., ShieldsZhou, G. A., Chen, X., Cremonese, L., Och, L., et al. (2013a). Carbon and strontium isotope evolution of seawater across the ediacaran–cambrian transition: Evidence from the xiaotan section, NE yunnan, south China. *Precambrian Res.* 225, 128–147. doi:10.1016/j.precamres.2012.01.002

Li, S., Li, X., Wang, G., Liu, Y., Wang, Z., Wang, T., et al. (2019b). Global Meso–Neoproterozoic plate reconstruction and formation mechanism for Precambrian basins: Constraints from three cratons in China. *Earth–Science Rev.* 198, 102946. doi:10.1016/j.earscirev.2019.102946

Li, Y. Q., He, D. F., and Wen, Z. (2013b). Palaeogeography and tectonic–depositional environment evolution of the Late Sinian in Sichuan Basin and adjacent areas. *J. Palaeogeogr.* 15, 231–245. doi:10.7605/gdlxb.2014.04.037

Li, Z., Evans, D. A., and Halverson, G. P. J. S. G. (2013c). Neoproterozoic glaciations in a revised global palaeogeography from the breakup of Rodinia to the assembly of Gondwanaland. *Sediment. Geol.* 294, 219–232. doi:10.1016/j.sedgeo.2013.05.016

Li, Z. X., Bogdanova, S., Collins, A., Davidson, A., De Waele, B., Ernst, R., et al. (2008). Assembly, configuration, and break–up history of Rodinia: A synthesis. *Precambrian Res.* 160, 179–210. doi:10.1016/j.precamres.2007.04.021

Liu, S., Yang, Y., Deng, B., Zhong, Y., Wen, L., Sun, W., et al. (2021). Tectonic evolution of the Sichuan Basin, southwest China. *Earth–Science Rev.* 213, 103470. doi:10.1016/j.earscirev.2020.103470

Liu, X. M., Hardisty, D. S., Lyons, T. W., and Swart, P. K. (2019). Evaluating the fidelity of the cerium paleoredox tracer during variable carbonate diagenesis on the

Great Bahamas Bank. *Geochimica Cosmochimica Acta* 248, 25–42. doi:10.1016/j.gca.2018.12.028

Loyd, S. J., Marenco, P. J., Hagadorn, J. W., Lyons, T. W., Kaufman, A. J., Sour–Tovar, F., et al. (2012). Sustained low marine sulfate concentrations from the Neoproterozoic to the Cambrian: Insights from carbonates of northwestern Mexico and eastern California. *Earth Planet. Sci. Lett.* 339 (340), 79–94. doi:10.1016/j.epsl.2012.05.032

Maloof, A. C., Ramezani, J., Bowring, S. A., Fike, D. A., Porter, S. M., and Mazouad, M. (2010). Constraints on early Cambrian carbon cycling from the duration of the Nemakit–Daldynian–Tommotian boundary δ13C shift, Morocco. *Geology* 38, 623–626. doi:10.1130/g30726.1

Marshall, J. D. (1992). Climatic and oceanographic isotopic signals from the carbonate rock record and their preservation. *Geol. Mag.* 129, 143–160. doi:10.1017/s0016756800008244

McFadden, K. A., Huang, J., Chu, X., Jiang, G., Kaufman, A. J., Zhou, C., et al. (2008). Pulsed oxidation and biological evolution in the ediacaran doushantuo formation. *Proc. Natl. Acad. Sci. U. S. A.* 105, 3197–3202. doi:10.1073/pnas.0708336105

Meyer, M., Xiao, S., Gill, B. C., Schiffbauer, J. D., Chen, Z., Zhou, C., et al. (2014). Interactions between Ediacaran animals and microbial mats: Insights from Lamonte trevallis, a new trace fossil from the Dengying Formation of South China. *Palaeogeogr. Palaeoclimatol. Palaeoecol.* 396, 62–74. doi:10.1016/j.palaeo.2013.12.026

Palmer, M. R., and Edmond, J. M. (1989). The strontium isotope budget of the modern ocean. *Earth Planet. Sci. Lett.* 92, 11–26. doi:10.1016/0012-821x(89)90017-4

Paula–Santos, G. M., Babinski, M., Kuchenbecker, M., Caetano–Filho, S., Trindade, R. I., and Pedrosa–Soares, A. C. (2015). New evidence of an Ediacaran age for the Bambuí Group in southern São Francisco craton (eastern Brazil) from zircon U–Pb data and isotope chemostratigraphy. *Gondwana Res.* 28, 702–720. doi:10.1016/j.gr.2014.07.012

Peucker–Ehrenbrink, B., and Miller, M. W. (2006). Marine 87Sr/86 Sr record mirrors the evolving upper continental crust. *Geochimica Cosmochimica Acta* 70, A487. doi:10.1016/j.gca.2006.06.1437

Qian, Y., Chuanlong, M., Haiquan, Z., Qinyin, T., Xiaosong, X., and Jianfei, Y. J. A. P. S., 2011. Sedimentary evolution and reservoir distribution of northern upper Yangtze plate in sinian–early paleozoic. 27, 672–680.

Ren, Y., Zhong, D., Gao, C., Li, B., Cao, X., Wang, A., et al. (2019). The paleoenvironmental evolution of the cambrian longwangmiao formation (stage 4, toyonian) on the Yangtze platform, south China: Petrographic and geochemical constrains. *Mar. Petroleum Geol.* 100, 391–411. doi:10.1016/j.marpetgeo.2018.10.022

Richter, F. M., Rowley, D. B., DePaolo, D. J. J. E., and Letters, P. S. (1992). Sr isotope evolution of seawater: The role of tectonics. *Earth Planet. Sci. Lett.* 109, 11–23. doi:10.1016/0012-821x(92)90070-c

Riquier, L., Tribovillard, N., Averbuch, O., Devleeschouwer, X., and Riboulleau, A. (2006). The Late Frasnian Kellwasser horizons of the Harz Mountains (Germany): Two oxygen–deficient periods resulting from different mechanisms. *Chem. Geol.* 233, 137–155. doi:10.1016/j.chemgeo.2006.02.021

Sawaki, Y., Kawai, T., Shibuya, T., Tahata, M., Omori, S., Komiya, T., et al. (2010a). 87Sr/86Sr chemostratigraphy of neoproterozoic dalradian carbonates below the port askaig glaciogenic formation, scotland. *Precambrian Res.* 179, 150–164. doi:10.1016/j.precamres.2010.02.021

Sawaki, Y., Ohno, T., Tahata, M., Komiya, T., Hirata, T., Maruyama, S., et al. (2010b). The ediacaran radiogenic Sr isotope excursion in the doushantuo Formation in the three Gorges area, south China. *Precambrian Res.* 176, 46–64. doi:10.1016/j.precamres.2009.10.006

Schiffbauer, J. D., Huntley, J. W., Fike, D. A., Jeffrey, M. J., Gregg, J. M., and Shelton, K. L. (2017). Decoupling biogeochemical records, extinction, and environmental change during the Cambrian SPICE event. *Sci. Adv.* 3, e1602158. doi:10.1126/sciadv.1602158

Schiffbauer, J. D. (2016). Research FOCUS: The age of tubes: A window into biological transition at the precambrian–cambrian boundary. *Geology* 44, 975–976. doi:10.1130/focus112016.1

Schiffbauer, J. D., Xiao, S., Cai, Y., Wallace, A. F., Hua, H., Hunter, J., et al. (2014). A unifying model for Neoproterozoic–Palaeozoic exceptional fossil preservation through pyritization and carbonaceous compression. *Nat. Commun.* 5, 5754. doi:10.1038/ncomms6754

Schildgen, T. F., Cosentino, D., Frijia, G., Castorina, F., Dudas, F. Ö., Iadanza, A., et al. (2014). Sea level and climate forcing of the Sr isotope composition of late Miocene Mediterranean marine basins. *Geochem. Geophys. Geosyst.* 15, 2964–2983. doi:10.1002/2014gc005332

Shen, B., Dong, L., Xiao, S., and Kowalewski, M. J. S. (2008). The avalon explosion: Evolution of ediacara morphospace. *Science* 319, 81–84. doi:10.1126/science.1150279

Siebert, C., Nägler, T. F., von Blanckenburg, F., Kramers, J. D. J. E., and Letters, P. S. (2003). Molybdenum isotope records as a potential new proxy for paleoceanography. *Earth Planet. Sci. Lett.* 211, 159–171. doi:10.1016/s0012-821x(03)00189-4

Sperling, E. A., Wolock, C. J., Morgan, A. S., Gill, B. C., Kunzmann, M., Halverson, G. P., et al. (2015). Statistical analysis of iron geochemical data suggests limited late Proterozoic oxygenation. *Nature* 523, 451–454. doi:10.1038/nature14589

Taylor, S. R., and McLennan, S. M. (1985). *The continental crust: Its composition and evolution*. Oxford: Blackwell, 312.

Tostevin, R., Wood, R., Shields, G., Poulton, S., Guilbaud, R., Bowyer, F., et al. (2016). Low–oxygen waters limited habitable space for early animals. *Nat. Commun.* 7, 12818–12819. doi:10.1038/ncomms12818

Tribovillard, N., Algeo, T. J., Baudin, F., and Riboulleau, A. (2012). Analysis of marine environmental conditions based onmolybdenum–uranium covariation—applications to mesozoic paleoceanography. *Chem. Geol.* 324–325, 46–58. doi:10.1016/j.chemgeo.2011.09.009

Tribovillard, N., Algeo, T. J., Lyons, T., and Riboulleau, A. (2006). Trace metals as paleoredox and paleoproductivity proxies: An update. *Chem. Geol.* 232, 12–32. doi:10.1016/j.chemgeo.2006.02.012

Valladares, M., Ugidos, J., Barba, P., Fallick, A., and Ellam, R. J. P. R. (2006). Oxygen, carbon and strontium isotope records of Ediacaran carbonates in Central Iberia (Spain). *Precambrian Res.* 147, 354–365. doi:10.1016/j.precamres.2006.01.021

van Smeerdijk Hood, A., and Wallace, M. W. (2012). Synsedimentary diagenesis in a Cryogenian reef complex: Ubiquitous marine dolomite precipitation. *Sediment. Geol.* 255, 56–71. doi:10.1016/j.sedgeo.2012.02.004

Veizer, J., Ala, D., Azmy, K., Bruckschen, P., Buhl, D., Bruhn, F., et al. (1999). 87Sr/86Sr, δ13C and δ18O evolution of Phanerozoic seawater. *Chem. Geol.* 161, 59–88. doi:10.1016/s0009-2541(99)00081-9

Wang, W., Pang, X., Chen, Z., Chen, D., Wang, Y., Yang, X., et al. (2021). Quantitative evaluation of transport efficiency of fault–reservoir composite migration pathway systems in carbonate petroliferous basins. *Energy* 222, 119983. doi:10.1016/j.energy.2021.119983

Wei, G., Ling, H., Shields, G. A., Chen, T., Lechte, M., Chen, X., et al. (2019). Long–term evolution of terrestrial inputs from the Ediacaran to early Cambrian: Clues from Nd isotopes in shallow–marine carbonates, South China. *Palaeogeogr. Palaeoclimatol. Palaeoecol.* 535, 109367. doi:10.1016/j.palaeo.2019.109367

Wei, G.–Y., Planavsky, N. J., Tarhan, L. G., He, T., Wang, D., Shields, G. A., et al. (2020). Highly dynamic marine redox state through the Cambrian explosion highlighted by authigenic δ238U records. *Earth Planet. Sci. Lett.* 544, 116361. doi:10.1016/j.epsl.2020.116361

Wood, R. A., Poulton, S. W., Prave, A. R., Hoffmann, K. H., Clarkson, M. O., Guilbaud, R., et al. (2015). Dynamic redox conditions control late Ediacaran metazoan ecosystems in the Nama Group, Namibia. *Precambrian Res.* 261, 252–271. doi:10.1016/j.precamres.2015.02.004

Yang, C., Li, X. H., Zhu, M., and Condon, D. J. (2017). SIMS U–Pb zircon geochronological constraints on upper Ediacaran stratigraphic correlations, South China. *Geol. Mag.* 154, 1202–1216. doi:10.1017/s0016756816001102

Zhang, F. F., Xiao, S. H., Kendall, B., Romaniello, S. J., Cui, H., Meyer, M., et al. (2018). Extensive marine anoxia during the terminal Ediacaran Period. *Sci. Adv.* 4, eaan8983. doi:10.1126/sciadv.aan8983

Zhang, P., Wang, Y., Zhang, X., Wei, Z., Wang, G., Zhang, T., et al. (2022). Carbon, oxygen and strontium isotopic and elemental characteristics of the Cambrian Longwangmiao Formation in South China: Paleoenvironmental significance and implications for carbon isotope excursions. *Gondwana Res.* 106, 174–190. doi:10.1016/j.gr.2022.01.008

Zhang, S., Jiang, G., Zhang, J., Song, B., Kennedy, M. J., and Christie–Blick, N. J. G. (2005). U–Pb sensitive high–resolution ion microprobe ages from the Doushantuo Formation in south China: Constraints on late Neoproterozoic glaciations. *Geol.* 33, 473–476. doi:10.1130/g21418.1

Zhang, T., Kershaw, S., Wan, Y., and Lan, G. (2000). Geochemical and facies evidence for palaeoenvironmental change during the late ordovician hirnantian glaciation in south sichuan province, China. *Glob. Planet. Change* 24, 133–152. doi:10.1016/s0921-8181(99)00063-6

10.3389/feart.2022.865709

Zhang, Y., Yang, T., Hohl, S. V., Zhu, B., He, T., Pan, W., et al. (2020). Seawater carbon and strontium isotope variations through the late Ediacaran to late Cambrian in the Tarim Basin. *Precambrian Res.* 345, 105769. doi:10.1016/j.precamres.2020.105769

Zhang, Y., Yin, L., Xiao, S., and Knoll, A. H. (1998). Permineralized fossils from the terminal proterozoic doushantuo formation south China. *J. Paleontol.* 72 (4), 1–52.

Zhao, Y., Zheng, Y., and Chen, F. (2009). Trace element and strontium isotope constraints on sedimentary environment of Ediacaran carbonates in southern Anhui, South China. *Chem. Geol.* 265, 345–362. doi:10.1016/j.chemgeo.2009.04.015

Zheng, D., Pang, X., Luo, B., Chen, D., Pang, B., Li, H., et al. (2021). Geochemical characteristics, genetic types, and source of natural gas in the Sinian Dengying Formation, Sichuan Basin, China. *J. Pet. Sci. Eng.* 199, 108341. doi:10.1016/j.petrol.2020.108341

Zhu, M., Strauss, H., and Shields, G. A. (2007a). From snowball earth to the cambrian bioradiation: Calibration of ediacaran–cambrian earth history in south China. *Palaeogeogr. Palaeoclimatol. Palaeoecol.* 254, 1. doi:10.1016/j.palaeo.2007.03.026

Zhu, M. Y., Babcock, L. E., and Peng, S. C. (2006). Advances in Cambrian stratigraphy and paleontology: Integrating correlation techniques, paleobiology, taphonomy and paleoenvironmental reconstruction. *Palaeoworld* 15, 217–222. doi:10.1016/j.palwor.2006.10.016

Zhu, M., Zhang, J., and Yang, A. (2007b). Integrated ediacaran (sinian) chronostratigraphy of South China. *Palaeogeogr. Palaeoclimatol. Palaeoecol.* 254, 7–61. doi:10.1016/j.palaeo.2007.03.025